ACS APPLIED MATERIALS & INTERFACES
Research Article
www.acsami.org

In Situ PL and SPV Monitored Charge Carrier Injection During Metal Assisted Etching of Intrinsic a-Si Layers on c-Si

Stefanie M. Greil,[†] Jörg Rappich,*[,†] Lars Korte,[†] and Stéphane Bastide[‡]

[†]Helmholtz-Zentrum Berlin für Materialien und Energie GmbH, Institut für Silizium-Photovoltaik, Kekuléstrasse 5, D-12489 Berlin, Germany

[‡]Institut de Chimie et des Matériaux Paris-Est—CMTR, CNRS, 2-8, rue H. Dunant, 94320 Thiais, France

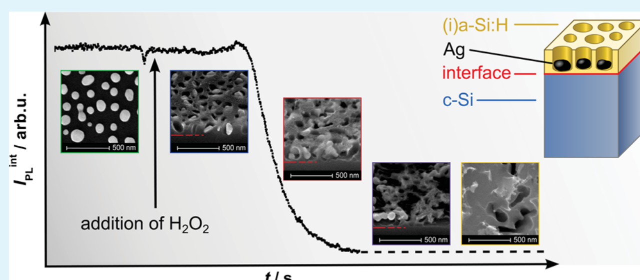

ABSTRACT: Although hydrogenated amorphous silicon is already widely examined regarding its structural and electronic properties, the chemical etching behavior of this material is only roughly understood. We present a detailed study of the etching properties of intrinsic hydrogenated amorphous silicon, (i)a-Si:H, layers on crystalline silicon, c-Si, within the framework of metal assisted chemical etching (MACE) using silver nanoparticles (Ag NPs). The etching processes are examined by *in situ* photoluminescence (PL) and *in situ* surface photovoltage (SPV) measurements, as these techniques allow a monitoring of the hole injection that takes place during MACE. By *in situ* PL measurements and SEM images, we could interpret the different stages of the MACE process of (i)a-Si:H layers and determine etch rates of (i)a-Si:H, that are found to be influenced by the size of the Ag NPs. *In situ* PL and *in situ* SPV measurements both enable researchers to determine when the Ag NPs reach the (i)a-Si:H/c-Si interface. Furthermore, a preferential MACE of (i)a-Si:H versus c-Si is revealed for the first time. This effect could be explained by an interplay of the different thermodynamic and structural properties of the two materials as well as by hole injection during MACE resulting in a field effect passivation. The presented results allow an application of the examined MACE processes for Si nanostructuring applications.

KEYWORDS: *amorphous silicon, preferential etching, metal assisted chemical etching, in situ photoluminescence, in situ surface photovoltage*

■ INTRODUCTION

Metal assisted chemical etching (MACE) is an outstanding tool for a variety of crystalline silicon (c-Si) nanostructuring processes.[1] It relies on the use of noble metal nanoparticles (NPs) acting as catalysts in HF solutions in the presence of an oxidizing agent (e.g., H_2O_2). Highly localized Si etching occurs around the NPs and results in the digging of well-defined mesopores with diameters closely matching that of the NPs. In the field of photovoltaics, MACE has been investigated as an alternative texturization treatment[2−4] for the elaboration of c-Si nanowire array based solar cells and the metallization of SiN_x:H and SiO_x dielectrics.[5]

While MACE of c-Si has been studied extensively in recent years, there is only one report regarding amorphous silicon (a-Si) by Chang et al.[6] They performed MACE with Au NPs and Au meshes on 1.2 μm thick a-Si layers which have been prepared by e-beam evaporation on c-Si at room temperature (yielding a low density a-Si). The etch rate of a-Si was found to be 3 times higher than that of polycrystalline Si under the same conditions. However, the etching features and mechanisms that govern MACE in this material are still unknown and hence constitute a field of investigation.

Here we present the first results on the application of MACE to the nanostructuring of intrinsic amorphous hydrogenated silicon, (i)a-Si:H layers used in heterojunction solar cells. We have investigated if highly localized etching of mesopores with metal nanoparticles could be performed in (i)a-Si:H layers similarly to c-Si in order to create nanometer-sized punctual openings through the amorphous layer that could be beneficial for the design of new cell architectures.[7] We used *in situ* photoluminescence (PL) excited in the underlying c-Si substrate and *in situ* surface photovoltage (SPV) to follow the etching process.[8] *In situ* PL is able to reveal photocarrier recombination and carrier injection into the c-Si substrate[9−12] and hence to follow the NPs' progressive motion through the (i)a-Si:H layer. New results have been obtained on etch rates in (i)a-Si:H, and a preferential etching of (i)a-Si:H versus c-Si is revealed by SEM studies.

■ EXPERIMENTAL SECTION

For all experiments, polished n-type float zone c-Si wafers, (100) and (111)-oriented, with a specific resistance of 1−10 Ωcm were used. The samples were cleaned by RCA process and HF-dipped before the deposition of a 100 nm thick (i)a-Si:H layer on the front side of the c-

Received: April 3, 2015
Accepted: May 12, 2015
Published: May 12, 2015

ACS Publications © 2015 American Chemical Society

DOI: 10.1021/acsami.5b02922
ACS Appl. Mater. Interfaces 2015, 7, 11654−11659

Si. To improve the photoluminescence intensity, the rear side of all c-Si samples was passivated by a 50 nm thick (i)a-Si:H layer.

The silver nanoparticles (Ag NPs) were prepared by dewetting of 10 or 20 nm thick Ag films deposited on the front sides of the native oxide covered (i)a-Si:H/c-Si samples and subsequent annealing under nitrogen flux at 220 °C for 10−20 min. To reach lower Ag coverage (below 10%), Ag evaporation through a mask of 200 nm polystyrene (PS) beads assembled in a compact array on the sample surface has also been performed.[13] After removing the PS beads by simple sonication in water, an annealing at 220 °C for 15 min was applied, leading to well-defined Ag NPs with a rounded shape.

Before the etching experiments, the samples with Ag NPs were placed in 1 M aqueous HF solution. The etching process was started by the addition of hydrogen peroxide, H_2O_2. The resulting H_2O_2 concentration in the solution was 5 mM. All solutions were prepared with chemicals of VLSI quality and Millipore water (18.2 MΩ cm).

For the *in situ* PL experiments, the samples were etched in an O-ring sealed cell, where the (i)a-Si:H side of the sample covered with Ag NPs was exposed to the etchant. The *in situ* PL measurements were performed through the electrolyte. A pulsed laser diode (Laser Components, iRLM-150-100-5324, λ_{ex} = 910 nm, τ_{pulse} = 100 ns) with a pulse energy of 6 μJ and a spot size of about 4 mm^2 with a diameter of 2.2 mm was used for the excitation. An influence of the photoinduced charge carriers on the etching process can be neglected since the light/dark ratio of the laser was 2×10^{-7} (two pulses per second). The integrated PL intensity I_{PL}^{int} of c-Si was measured by means of an InGaAs time integrating detector using an interference filter with a transmission maximum at 1130 nm. The *in situ* PL setup was already described elsewhere.[8,14]

Additionally, *in situ* surface photovoltage (SPV) at the (i)a-Si:H/c-Si−electrolyte interface of the etched sample was measured simultaneously with PL using the same excitation pulse.[9,15]

For further investigation of the MACE process, *in situ* reflectance measurements were carried out using a Lambda 19 UV−vis spectrometer from PerkinElmer. The (i)a-Si:H/c-Si samples were placed in a cuvette with 1 M HF solution so that the incoming light was perpendicular to the sample surface. Again, the etching process was started by the addition of H_2O_2 (5 mM), and the reflectance was measured at 910 nm as a function of time.

Scanning electron microscopy (SEM) images of the surfaces (plane view) and the interfaces (cross section) were obtained with a Hitachi S-4100 system using a cold field emission cathode as electron source. The Ag NP characteristics (size, morphology, coverage) were analyzed from SEM images in plane view with the software ImageJ. The characteristics given hereafter correspond to average values over a large number of NPs, from 50 to 400 depending on the Ag coverage.

RESULTS

Ag NP Formation and Characteristics. Ag NPs prepared by the dewetting method of a 10 nm thick Ag layer on (i)a-Si:H/c-Si substrates at 220 °C are shown in the top view SEM image (A) of Figure 1b. They mostly exhibit a rounded shape with, in this particular case, an average Feret diameter, circularity, and coverage of 126 nm, 0.81, and 26%, respectively. The NP characteristics can be modified by changing the Ag layer thickness and/or the dewetting time (see Experimental Section). In the present work, the Ag NP Feret diameter was varied from 80 to 900 nm. With increasing size, the Ag NPs tend to adopt an elongated rather than rounded shape, which is the reason they are characterized by their maximum Feret diameter (longest distance between two points of the boundary). The Ag coverage varies from 4% to 40%, depending on the amount of evaporated Ag, the annealing time, and the use of a PS bead mask (necessary to achieve low coverage, see Experimental Section).

Changes in PL of c-Si During MACE. Measuring *in situ* the PL of c-Si allows researchers to probe the recombination processes occurring at the (i)a-Si:H/c-Si interface during etching. The evolution of I_{PL}^{int} as a function of time is reported in Figure 1a. First, the sample is in contact with the 1 M HF solution (A). The initial I_{PL}^{int} value is about 4.1 (arbitrary units). MACE is started by the addition of H_2O_2 at $t = 0$ s. I_{PL}^{int} does not change with the onset of the MACE process (B), but a small increase (∼5%) occurs after around 80 s (C), followed by a steep reduction in I_{PL}^{int} with further etching (D), where obviously a large amount of defects at the (i)a-Si:H/c-Si interface is created. The final value, 1.1 (arbitrary units), corresponds to a reduction of I_{PL}^{int} by 75%.

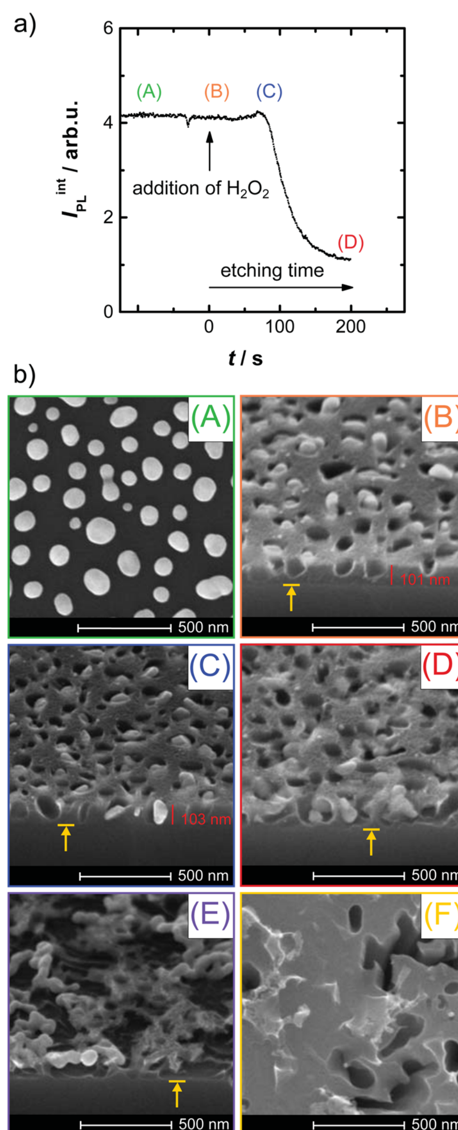

Figure 1. (a) *In situ* PL measured in aqueous HF solution before and after the injection of the oxidizing agent (H_2O_2); (b) SEM images obtained before (A) and after etching for (B) 55 s, (C) 95 s, (D) 250 s, (E) 500 s, and (F) > 15 min. The yellow arrows locate the (i)a-Si:H/c-Si interface.

Surface and Interface Morphology. The SEM images (A−F) of Figure 1b correspond to samples for which the etching was stopped at the different stages indicated on the I_{PL}^{int} curve. First of all, image B shows that MACE in (i)a-Si:H results in a highly localized dissolution around the Ag NPs, similar to the case of c-Si. The pore openings match the NP diameter within a few nanometers. Cross sectional SEM

observations also inform on the Ag NP position with respect to the (i)a-Si:H/c-Si interface (indicated by an arrow in the images): when MACE is stopped after 55 s (B), the Ag NPs are located within the (i)a-Si:H layer whereas after 95 s, before the strong decrease in I_{PL}^{int} (C), the Ag NPs have just reached the (i)a-Si:H/c-Si interface. We therefore assume that the decrease in I_{PL}^{int} results from the creation of nonradiative surface defects when the interface (i.e., the c-Si substrate) is reached by the Ag NPs.

Interestingly, SEM images obtained after etching times of 250 s (D) and 500 s (E) reveal a preferential etching of the (i)a-Si:H layer. Indeed, the Ag NPs continue to etch the (i)a-Si:H layer laterally instead of penetrating into the c-Si substrate. After 500 s, most of the (i)a-Si:H layer is etched, whereas the c-Si substrate remains nearly untouched. For considerably longer etching times (>15 min), Ag NPs cluster to larger conglomerates and start etching the c-Si substrate (see Figure 1b, image F).

Changes in Reflectivity During Etching. Beside recombination, another parameter can affect I_{PL}^{int}, the surface reflectivity. Etching with Ag NPs creates mesopores that result in a top layer with an effective refractive index (combination of the refractive indices of the solution in the mesopores and of the (i)a-Si:H). This can reduce the reflectivity due to an increase in the amount of excitation light coupled into the substrate, as well as the transmission of PL outside the sample,[16] and consequently influence I_{PL}^{int}. Additionally, the presence of the Ag NPs at the bottom of the mesopores may also affect the reflectivity in a way that is difficult to assess, since antireflection coating effects and/or plasmonic effects can come into play.[17]

We have therefore measured the time evolution of the reflectivity of (i)a-Si:H/c-Si samples during a MACE process at the excitation wavelength used for PL (910 nm) by *in situ* UV−vis spectroscopy, as presented in Figure 2. The initial reflectivity

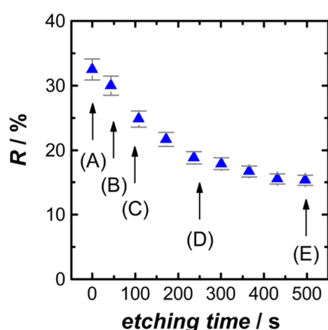

Figure 2. Evolution of the reflectivity of an (i)a-Si:H/c-Si sample measured *in situ* during MACE as a function of time. The arrows correspond to the etching times of samples (A−E).

of the sample decreases by 24% during the first 100 s of etching, corresponding to 10% additional light in the sample, but I_{PL}^{int} remains stable or slightly increases (5%). The reflectivity further decreases markedly by 45% and 54% after 250 and 500 s, respectively. However, I_{PL}^{int} does not rise as a result of this reduction in reflectivity. It seems that the deleterious effect of nonradiative surface states created at the (i)a-Si:H/c-Si interface largely outcomes the changes in reflectivity.

Etch Rates of a-Si:H Layer on c-Si. From SEM and PL measurements displayed in Figure 1, the etch rate of (i)a-Si:H by the Ag NPs is calculated to be ∼1.6 nm s^{-1}. However, we have found that it strongly depends on the Ag NP characteristics. Figure 3a plots the etch rates of (i)a-Si:H as a function of the Ag NP Feret diameter (top) together with the Ag coverage (bottom). The graphs indicate that the etch rate is roughly inversely proportional to the Ag NP size. In addition, the Ag coverage seems to have some influence on the spread of etch rates. Therefore, the etch rates are normalized by (1 − "Ag coverage"), a measure of the free area surrounding Ag NPs, and plotted versus the Ag NP Feret diameter in Figure 3b. In this way, a more linear variation of etch rates with the Ag NP Feret diameter is obtained, except for the sample which presents both the lowest Ag coverage and the smallest diameter.

In a comparison to c-Si, (i)a-Si:H is found to be etched about 2 times faster under the same conditions (data for c-Si not shown here). This is in agreement with a previous report regarding MACE performed with Au meshes, where Chang et al. have established a ratio of 3 between the etch rates of a-Si and polycrystalline Si.[6]

We have also carried out etching of (i)a-Si:H in $HF-H_2O_2$ without Ag NPs (homogeneous layer etching). The evolution of I_{PL}^{int} is similar to that obtained with Ag NPs, but the period of time before the strong reduction of I_{PL}^{int} is much longer, corresponding to an etch rate of ∼0.13 nm s^{-1}.

***In Situ* Surface Photovoltage of the c-Si.** SPV was also measured *in situ* during the etching process simultaneously to PL, as shown in Figure 4a. Just after the addition of H_2O_2, the so far stable SPV (in 1 M HF) slightly decreases before exhibiting a strong increase concomitant to the drop of I_{PL}^{int}. Hence, an increase in the band bending of c-Si at the (i)a-Si:H/c-Si interface occurs when the Ag NPs reach the interface (label C).

Surface Passivation as a Function of Etched Area/Ag Coverage. MACE with Ag NPs is intended to realize local nano-openings in the (i)a-Si:H layer, allowing electrical contacts on c-Si while preserving the passivating (i)a-Si:H layer everywhere else. An SEM image of such nano-openings is provided in Figure 4c for a sample with 85 nm Ag NPs at low coverage (4.1%). The level of surface passivation maintained after MACE can be evaluated from the evolution of I_{PL}^{int}. In Figure 5, the reduction in I_{PL}^{int} (final vs initial value) is plotted as a function of the etched area, which corresponds to the Ag coverage (the sample with a 100% etched area was however obtained in $HF-H_2O_2$ without Ag NPs, in order to achieve a homogeneous and complete removal of the (i)a-Si:H layer).

Under full etching of the (i)a:Si-layer, the surface passivation is reduced by more than 80% of its initial value. As could be expected, a restriction of the etched area by MACE with Ag NPs allows for maintenance of the passivation at a higher level. However, low Ag coverages (below 10%) are required to achieve a significant improvement (reduction of I_{PL}^{int} by less than 60%) compared to full layer etching.

■ DISCUSSION

Evolution of PL During MACE. The changes in I_{PL}^{int} during etching can be understood by considering the radiative (RR) and nonradiative (NRR) recombination processes in c-Si. As shown in Figure 6, I_{PL}^{int} is an indirect measure of the concentration of NRR active surface defects at the (i)a-Si:H/c-Si interface (D_{it}).[18]

A reduction in I_{PL}^{int} corresponds to an increase in the number of NRR active interface defects of c-Si at the (i)a-Si:H/c-Si interface.[11] This happens when the (i)a-Si:H passivation is

DOI: 10.1021/acsami.5b02922
ACS Appl. Mater. Interfaces 2015, 7, 11654−11659

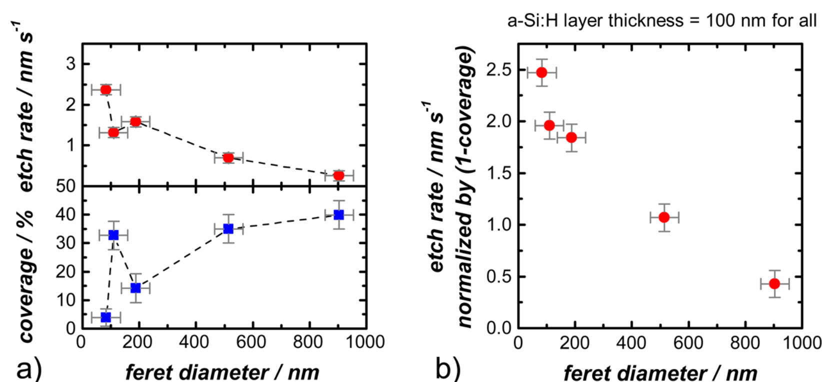

Figure 3. (a) MACE etch rates of (i)a-Si:H and the corresponding Ag coverage of different (i)a-Si:H/c-Si samples after the MACE process versus the Feret diameter of Ag NPs. (b) Etch rates of (i)a-Si:H normalized by (1 − "Ag coverage").

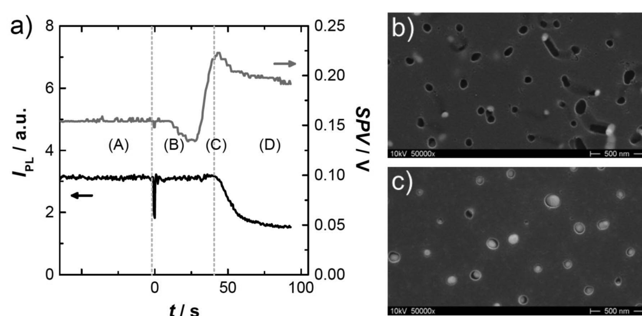

Figure 4. (a) Graphs: simultaneous measurements of *in situ* PL (black line) and *in situ* SPV (gray line) during MACE of a (i)a-Si:H/c-Si sample. The labels A−D correspond to the stages described in Figure 1. (b) SEM image of the surface of the corresponding sample after etching. (c) SEM image where etching was stopped at point C.

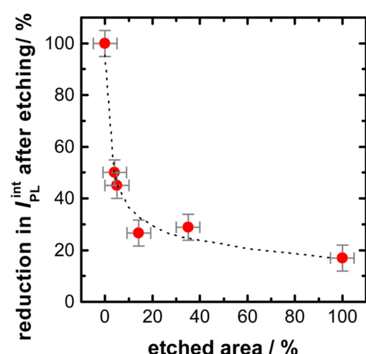

Figure 5. Reduction in I_{PL}^{int} by MACE with Ag NPs as a function of the etched area, i.e., the Ag coverage (except at 100%, see text). The dotted line is a guide for the eyes.

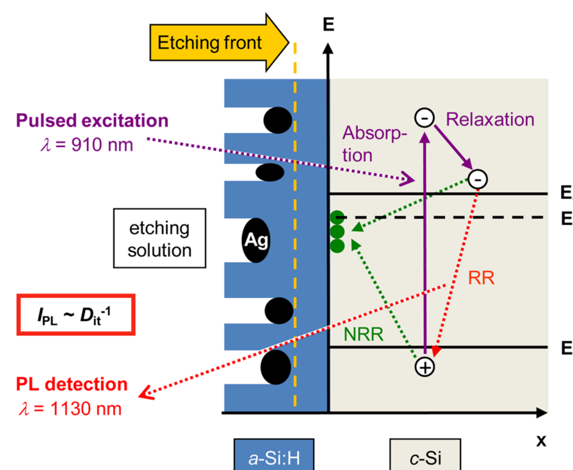

Figure 6. Radiative (RR) and nonradiative (NRR) recombination processes during etching of an a-Si:H layer on c-Si by Ag NPs in HF-H_2O_2.

locally destroyed, i.e., when the generation of NRR active interface defects at the c-Si surface starts due to Si−Si bond breaking.[8,14] Therefore, the beginning of the decrease in I_{PL}^{int} can be assigned to the state when Ag NPs reach the (i)a-Si:H/c-Si interface (stage C in Figure 1). I_{PL}^{int} further decreases during ongoing etching and stabilizes (at longer etching times). However, I_{PL}^{int} does not decrease to very low values during MACE as it is obtained for etch-back of full area (i)a-Si:H layers on c-Si substrates.[11] The value of I_{PL}^{int} after etching correlates to the area fraction of the remaining passivating (i)a-Si:H layer; i.e., it increases when the etched area decreases (cf., Figure 5). However, I_{PL}^{int} after etching is not linearly proportional to the fraction of unetched surface area, and even at the lowest coverage, ∼4%, I_{PL}^{int} is reduced by 50%. These results are in accordance with Schöfthaler et al., who showed that the effective lifetime of Si wafer with Ag point contacts decreases exponentially with increasing metallization ratio of the wafer surface.[19] The broadening of the decrease in PL is due to the size distribution of the Ag NPs which have different etching rates and therefore reach the c-Si surface at different times. As shown by the SEM image in Figure 4, it is clear though that the etching time was longer than necessary to simply open the (i)a-Si:H layer, resulting in unnecessary removal of (i)a-Si:H due to lateral etching. The etched area is then slightly higher than the 4% estimated from the Ag coverage. However, in Figure 4c, an SEM image of a sample where the MACE process was stopped at stage C is depicted. It shows that the MACE process can be controlled very well by *in situ* PL measurements to create well-defined nano-openings in the (i)a-Si:H layer without any lateral etching.

Evolution of SPV During MACE. As for I_{PL}^{int}, it is possible to relate the evolution of SPV to the Ag NP location during etching. As long as the Ag NPs are embedded in the (i)a-Si:H layer, the band bending remains stable, as schematized in Figure 7a. We can assume that hole injection from the Ag NPs is confined in (i)a-Si:H because of it is high bulk defect density (>10^{17} cm^{-3} for the used (i)a-Si:H). However, when they reach the (i)a-Si:H/c-Si interface, holes can be injected directly into the valence band of c-Si.[20] For the n-doped Si substrates used,

DOI: 10.1021/acsami.5b02922
ACS Appl. Mater. Interfaces 2015, 7, 11654−11659

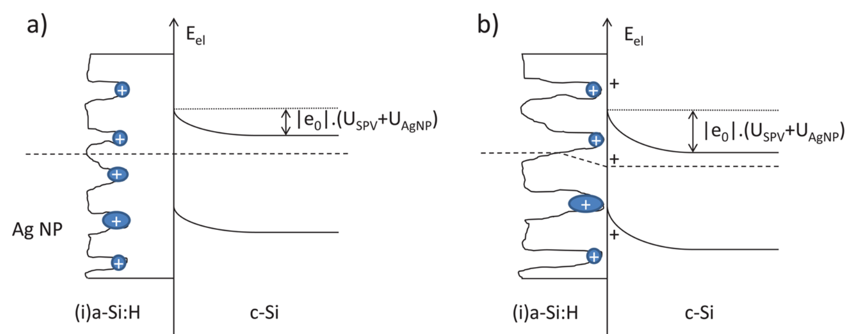

Figure 7. Change in surface photovoltage, SPV ($=|e_0| \cdot [U_{SPV} + U_{AgNP}]$), during MACE of (i)a-Si:H/c-Si samples due to hole injection. (a) MACE is taking place within the (i)a-Si:H layer. Injected holes by Ag NPs directly recombine within the (i)a-Si:H layer. (b) MACE and the Ag NPs reach the (i)a-Si:H/c-Si interface, and hole injection directly into the valence band of c-Si is taking place, leading to a pronounced increase in surface photovoltage.

an injection of holes should lead to a further depletion of electrons at the (i)a-Si:H/c-Si interface, and therefore to an enhancement in the band bending of n-doped c-Si[12] as schemed in Figure 7b. This is in agreement with the observed large increase of SPV. Therefore, the state when the Ag NPs reach the (i)a-Si:H/c-Si interface can be monitored distinctly by the *in situ* SPV measurement shown in Figure 4. The enhanced band bending normally results in a field effect passivation that can lead to an increase in the PL intensity, as already reported for bare c-Si etching in HF-HNO_3.[12] We have actually observed this passivation effect for MACE with Ag NPs performed on bare c-Si (i.e., without passivation). Right after the addition of H_2O_2, I_{PL}^{int} increases by a factor 2 for a few tens of seconds before going back to lower values. However, the (i)a-Si:H layer in the present samples already ensures a good passivation and makes this field effect passivation almost indistinguishable. (A small increase of I_{PL}^{int} just before stage C in Figures 1 and 4 is visible though, but could also be related to the lowering of the reflectivity.)

Preferential Etching of (i)a-Si:H versus c-Si. The discovered preferential etching of (i)a-Si:H versus c-Si occurring during MACE is a result of the interplay of the differences in thermodynamic properties of a-Si:H and c-Si and the characteristics of the MACE process. Amorphous Si possesses a more positive standard enthalpy of formation than that of c-Si[21] and is therefore thermodynamically preferentially dissolved. Furthermore, structural aspects of (i)a-Si:H play a role for the preferred etching, since the higher structural disorder in (i)a-Si:H facilitates the dissolution process by HF molecules of the catalytically oxidized Si surface atoms (by the injected holes).[22,23] Additionally, the Ag NPs are temporarily positively charged during the MACE process.[24] Due to this positive charge, the Ag NPs are slightly repelled by the also positively charged n-type Si substrate. In (i)a-Si:H, a surface band bending cannot be established because (i)a-Si:H presents a significantly higher defect density than c-Si.[25] Preferential etching of the (i)a-Si:H layer is supported by the fact that Ag NPs are to a certain extent able to move during MACE.[26] The Ag NPs exhibit a movement parallel to the (i)a-Si:H/c-Si interface leading to a formation of Ag NP clusters (see SEM images of Figures 1b, images D and E). As soon as the formed Ag NP clusters have become large enough, they lose their ability of lateral movement[27] and start etching c-Si perpendicularly, as shown in Figure 1b, image F.

Etch Rate as a Function of the Feret Diameter of Ag NPs. The linear variation of the normalized etch rate of (i)a-Si:H, inversely proportional to the Feret diameter of Ag NPs (Figure 3a), may be the result of the HF diffusion toward the Ag NP/(i)a-Si:H interface, via first Fick's law, to dissolve oxidized Si surface atoms after hole injection from the Ag NPs. The larger the Feret diameter, the longer the time needed for the HF species to diffuse to the oxidized (i)a-Si:H species. This is also reflected by plotting the normalized etch rate versus the Ag NPs' Feret diameter (Figure 3b); it linearly decreases with increasing area of the Feret diameter of the Ag NPs. We believe that this result is of general interest in MACE of Si with metal NPs, as suggested by Huang et al. in their review on this research field.[1]

The linear variation obtained by normalizing with (1− Ag coverage) indicates that the etch rate is also affected by the "free" area between Ag NPs, in the sense that the etching current decreases when Ag NPs get closer. In the field of microelectrode arrays, it is well-established that the distance between microelectrodes is a key parameter:[28] if it is large enough so that each electrode in the array acts as an individual microelectrode, a maximum current is achieved (radial diffusion); if the spacing is reduced, the adjacent diffusion zones overlap, depleting the same region of solution and the current decreases for each microelectrode (planar diffusion as limiting case). A more detailed analysis would be beyond the scope of this work, but we assume that the normalization allows us to roughly take into account the influence of the distance between Ag NPs on etch rates, except apparently for the sample with the lowest coverage and smallest NP size.

For a-Si:H, the alloy composition, as hydrogen content, bonding configurations, and the Fermi level position, which depends on doping level and defect density, may affect the etching properties. Furthermore, the microstructure of a-Si:H alloys, such as voids, columnar growth structure, micro-crystallinity, etc., may also influence the etching properties.[29] In this study, these influences are assumed to be constant since the deposition of the (i)a-Si:H layers was done under exactly the same conditions, but they constitute an interesting aspect to explore in a future work.

■ CONCLUSION

We have carried out a detailed study on MACE of (i)a-Si:H layers deposited on c-Si with Ag NPs of various size and surface coverage. The results show that the etching process can be followed and controlled by *in situ* photoluminescence as well as by *in situ* surface photovoltage techniques, thanks to their sensitivity to hole injection into c-Si during MACE. With this

ability of control, etching can be carried out exactly to the (i)a-Si:H/c-Si interface (stage C in Figure 1), which is essential for minimizing etching induced defects.

A preferential MACE of (i)a-Si:H versus c-Si is observed for the first time. After having reached the (i)a-Si:H/c-Si interface, the Ag NPs change the etching direction to perform lateral etching of the (i)a-Si:H layer instead of continuing digging mesopores into c-Si. This preferred etching of (i)a-Si:H may be the result of (I) the different structural and thermodynamic properties of (i)a-Si:H and c-Si and (II) the formation of a field effect passivation due to the hole injection into c-Si during MACE, that leads to a repulsion of the positively charged Ag NPs from the interface.

Additionally, we found that, besides the concentrations of H_2O_2 and HF, the etch rate of (i)a-Si:H also depends on the Feret diameter of the Ag NPs as well as on the distance between them.

This work demonstrates that MACE with Ag NPs can be used to create nanometer-sized punctual openings through passivating (i)a-Si:H layers that could be useful for the design of new solar cell contact architectures with improved surface passivation properties. The presented MACE process is now able to replace the complex photolithography processing for the formation of point contacted silicon heterojunction solar cells by profiting from the highly effective control of *in situ* surface photovoltage or more important of the contactless *in situ* photoluminescence measurements.

■ AUTHOR INFORMATION

Corresponding Author

*E-mail: rappich@helmholtz-berlin.de.

Notes

The authors declare no competing financial interest.

■ ACKNOWLEDGMENTS

The authors like to thank E. Conrad, K. Jacob, and C. Klimm for assistance in preparation and characterization of the samples.

■ REFERENCES

(1) Huang, Z.; Geyer, N.; Werner, P.; de Boor, J.; Gösele, U. Metal-Assisted Chemical Etching of Silicon: A Review. *Adv. Mater.* **2011**, *23*, 285−308.

(2) Jia, G.; Eisenhawer, B.; Dellith, J.; Falk, F.; Thøgersen, A.; Ulyashin, A. Multiple Core−Shell Silicon Nanowire-Based Heterojunction Solar Cells. *J. Phys. Chem. C* **2013**, *117*, 1091−1096.

(3) Song, T.; Lee, S.-T.; Sun, B. Silicon Nanowires for Photovoltaic Applications: The Progress and Challenge. *Nano Energy* **2012**, *1*, 654−673.

(4) Bastide, S.; Quang, N. Le; Monna, R.; Lévy-Clément, C. Chemical Etching of Si by Ag Nanocatalysts in HF-H2O2: Application to Multicrystalline Si Solar Cell Texturisation. *Phys. Status Solidi* **2009**, *6*, 1536−1540.

(5) Bastide, S.; Nychyporuk, T.; Zhou, Z.; Fave, A.; Lemiti, M. Facile Metallization of Dielectric Coatings for Plasmonic Solar Cells. *Sol. Energy Mater. Sol. Cells* **2012**, *102*, 26−30.

(6) Chang, S.; Chuang, V. P.; Boles, S. T.; Thompson, C. V. Metal-Catalyzed Etching of Vertically Aligned Polysilicon and Amorphous Silicon Nanowire Arrays by Etching Direction Confinement. *Adv. Funct. Mater.* **2010**, *20*, 4364−4370.

(7) Haschke, J.; Mingirulli, N.; Rech, B. Progress in Point Contacted Rear Silicon Heterojunction Solar Cells. *Energy Procedia* **2012**, *27*, 116−121.

(8) Rappich, J.; Timoshenko, V.; Dittrich, T. In Situ Monitoring of Electrochemical Processes at the (100) p-Si/Aqueous NH4F Electrolyte Interface by Photoluminescence. *J. Electrochem. Soc.* **1997**, *144*, 493−496.

(9) Dittrich, T.; Burke, T.; Koch, F.; Rappich, J. Passivation of an Anodic Oxide/p-Si Interface Stimulated by Electron Injection. *J. Appl. Phys.* **2001**, *89*, 4636−4642.

(10) Yahyaoui, F.; Dittrich, T.; Burke, T.; Aggour, M.; Lust, S.; Lévy-Clément, C.; Rappich, J. Band Bending and Nonradiative Recombination at Si Surfaces during Electrochemical Treatment in Aqueous Fluoride Solution. *J. Electrochem. Soc.* **2002**, *149*, E472−E478.

(11) Greil, S. M.; Mingirulli, N.; Korte, L.; Hartmann, K.; Schöpke, A.; Rappich, J.; Rech, B. Etching of a-Si:H on c-Si Absorber Monitored by In Situ Photoluminescence Measurements. *Energy Procedia* **2011**, *8*, 269−274.

(12) Greil, S.; Schöpke, A.; Rappich, J. Strongly Reduced Si Surface Recombination by Charge Injection during Etching in Diluted HF/HNO3. *ChemPhysChem* **2012**, *13*, 2982−2988.

(13) Hulteen, J. C.; Van Duyne, R. P. Nanosphere Lithography: A Materials General Fabrication Process for Periodic Particle Array Surfaces. *J. Vac. Sci. Technol., A* **1995**, *13* (3), 1553−1558.

(14) Rappich, J.; Dittrich, T. Electrochemical Passivation of Si and SiGe Surfaces. In *Thin Film Handbook*; Nalwa, H. S., Ed.; Academic Press: New York, 2002; pp 1−56.

(15) Yang, F.; Roodenko, K.; Hinrichs, K.; Rappich, J. Electronic and Surface Properties during the Etch-Back of Anodic Oxides on Si(111) Surfaces in 40% NH4F Solution. *J. Micromech. Microeng.* **2007**, *17*, S56−S60.

(16) Pillai, S.; Catchpole, K. R.; Trupke, T.; Zhang, G.; Zhao, J.; Green, M. A. Enhanced Emission from Si-Based Light-Emitting Diodes Using Surface Plasmons. *Appl. Phys. Lett.* **2006**, *88*, 161102.

(17) Ouyang, Z.; Zhao, X.; Varlamov, S.; Tao, Y.; Wong, J.; Pillai, S. Nanoparticle-Enhanced Light Trapping in Thin-Film Silicon Solar Cells. *Prog. Photovoltaics* **2011**, 917−926.

(18) Timoshenko, V. A.; Petrenko, A. B.; Stolyarov, M. N.; Fuessel, W.; Rappich, J. Quantitative Analysis of Room Temperature Photoluminescence of c-Si Wafers Excited by Short Laser Pulses. *J. Appl. Phys.* **1999**, *85*, 4171−4175.

(19) Schöfthaler, M.; Rau, U.; Werner, J. Direct Observation of a Scaling Effect on Effective Minority Carrier Lifetimes. *J. Appl. Phys.* **1994**, *76*, 4168−4172.

(20) Chartier, C.; Bastide, S.; Lévy-Clément, C. Metal-Assisted Chemical Etching of Silicon in HF−H2O2. *Electrochim. Acta* **2008**, *53*, 5509−5516.

(21) Donovan, E. P.; Spaepen, F.; Turnbull, D.; Poate, J. M.; Jacobson, D. C. Heat of Crystallization and Melting Point of Amorphous Silicon. *Appl. Phys. Lett.* **1983**, *42*, 698−700.

(22) Biswas, R.; Pan, B.; Ye, Y. Metastability of Amorphous Silicon from Silicon Network Rebonding. *Phys. Rev. Lett.* **2002**, *88*, 205502.

(23) Street, R. Hydrogen Diffusion and Electronic Metastability in Amorphous Silicon. *Phys. B (Amsterdam, Neth.)* **1991**, *170*, 69−81.

(24) Geyer, N.; Fuhrmann, B. Ag-Mediated Charge Transport during Metal-Assisted Chemical Etching of Silicon Nanowires. *ACS Appl. Mater. Interfaces* **2013**, *5*, 4302−4308.

(25) Street, R. Distribution of the Density of States of Bonded Hydrogen in Amorphous Hydrogenated Silicon. *Sol. Cells* **1991**, *30*, 207−218.

(26) Tsujino, K.; Matsumura, M. Morphology of Nanoholes formed in Silicon by Wet Etching in Solutions Containing HF and H2O2 at Different Concentrations using Silver Nanoparticles as Catalysts. *Electrochim. Acta* **2007**, *53*, 28−34.

(27) Milazzo, R. G.; D'Arrigo, G.; Spinella, C.; Grimaldi, M. G.; Rimini, E. Ag-Assisted Chemical Etching of (100) and (111) n-Type Silicon Substrates by Varying the Amount of Deposited Metal. *J. Electrochem. Soc.* **2012**, *159*, D521−D525.

(28) Davies, T. J.; Compton, R. G. The Cyclic and Linear Sweep Voltammetry of Regular and Random Arrays of Microdisc Electrodes: Theory. *J. Electroanal. Chem.* **2005**, *585*, 63−82.

(29) Tsuo, Y. S.; Xu, Y.; Baker, D. W.; Deb, S. K. Etching Properties of Hydrogenated Amorphous Silicon. *Mater. Res. Soc. Symp. Proc.* **1991**, *219*, 805−810.

DOI: 10.1021/acsami.5b02922
ACS Appl. Mater. Interfaces 2015, 7, 11654−11659